Available online at www.sciencedirect.com
ScienceDirect
International Journal of Heat and Mass Transfer 50 (2007) 151–162
International Journal of HEAT and MASS TRANSFER
www.elsevier.com/locate/ijhmt

Heat and mass transfer in a cross-flow membrane-based enthalpy exchanger under naturally formed boundary conditions

Li-Zhi Zhang *

Key Laboratory of Enhanced Heat Transfer and Energy Conservation of Education Ministry, School of Chemical and Energy Engineering, South China University of Technology, Guangzhou 510640, China

Received 28 October 2005; received in revised form 20 June 2006
Available online 1 September 2006

Abstract

Heat and mass transfer mechanisms in a cross-flow parallel plate membrane-based enthalpy exchanger for heat and moisture recovery from exhaust air streams are investigated. The flow is assumed laminar and hydrodynamically fully developed, but developing in thermal and concentration boundaries. Contrary to the traditional methods to assume a uniform temperature (concentration) or a uniform heat flux (mass flux) boundary condition, in this study, the real boundary conditions on the exchanger surfaces are obtained by the numerical solution of the coupled equations that govern the transfer of momentum, thermal energy, and moisture in the two cross-flow air streams and through the membrane. The naturally formed heat and mass boundary conditions are then used to calculate the local and mean Nusselt and Sherwood numbers along the cross-flow passages, in the developing region and thereafter. A comparison was made with those results under uniform temperature (concentration) and uniform heat flux (mass flux) boundary conditions, for rectangular ducts of various aspect ratios. An experiment is done to verify the prediction of outlet moisture content.

Keywords: Heat transfer; Mass transfer; Membranes; Boundary conditions; Cross-flow; Duct

1. Introduction

Conditioning ventilation air typically constitutes 20–40% of the thermal load for commercial buildings and can be even higher in buildings that require 100% outdoor air to meet ventilation standards [1]. Energy recovery devices could save a large fraction of the thermal load since heat and humidity would be recovered from the exhaust stream in winter and excess heat and moisture would be transferred to the exhaust in order to cool and dehumidify the incoming air (fresh) in the summer. Besides, with energy recovery devices, the efficiency of the existing HVAC systems can be improved because otherwise fresh air needs to be dehumidified by cooling coil through condensation followed by a re-heating process, which is very energy intensive.

The most common techniques [2–5] for energy recovery can be classified into two categories: sensible heat exchangers and energy wheels. Sensible exchangers, such as fixed plates, sensible heat exchange wheels, heat pipes, and coil run-around loop heat exchangers, can only recover sensible heat with no moisture recovery. Energy wheels, which recover both heat and moisture, have a higher effectiveness, thus are more attractive. However, energy wheels are very expensive and they have moving parts that may be problematic for maintenance. The carry-over is also a big problem.

In recent years, another technique that involves membrane technology has been investigated for possible energy recovery from exhaust air streams [6,7]. It is called the enthalpy exchanger with hydrophilic membrane cores. The device is just like an air-to-air sensible heat exchanger. But in place of traditional metal heat exchange plates, novel hydrophilic membranes, which can exchange both heat and moisture simultaneously, are used as the heat

* Tel./fax: +86 20 87114268.
E-mail address: Lzzhang@scut.edu.cn

0017-9310/$ - see front matter © 2006 Elsevier Ltd. All rights reserved.
doi:10.1016/j.ijheatmasstransfer.2006.06.025

Nomenclature

a	half duct height (m)
A_c	cross-section area (m^2)
AC	acetate cellulose
b	half duct width (m)
C	shape factor for the isotherm
c_p	specific heat (kJ kg^{-1} K^{-1})
D	diffusivity (m^2/s)
D_h	hydrodynamic diameter (m)
f	friction factor
h	convective heat transfer coefficient (kW m^{-2} K^{-1})
k	convective mass transfer coefficient (m/s)
Le	Lewis number
$\dot{m}_v$	local emission rate (kg m^{-2} s^{-1})
Nu	Nusselt number
P	pressure (Pa)
P_d	perimeter (m)
Re	Reynolds number
Pr	Prandtl number
RH	air relative humidity
Sc	Schmidt number
Sh	Sherwood number
T	temperature (K)
u	velocity (m/s)
W	water uptake (kg/kg)
W_{max}	maximum water uptake of membrane material (kg/kg)
x, y, z	coordinates (m)

Greek symbols

δ	membrane thickness (m)
μ	dynamic viscosity (Pa s)
ρ	density of dry air (kg/m^3)
ξ	dimensionless humidity
θ	dimensionless temperature
ω	humidity ratio (kg moisture/kg air)
λ	thermal conductivity (kW m^{-1} K^{-1})

Superscripts

*	dimensionless
′	exhaust air duct

Subscripts

1	fresh air side
2	exhaust air side
a	air
b	bulk
G	geometric
h	heat
i	inlet
L	local
m	mass, mean, membrane
o	outlet
s	surface
v	vapor

mass transfer media. Results found that compared to an energy wheel, it has the same even higher enthalpy effectiveness. Furthermore, the problem of carry-over could be prevented.

The enthalpy exchanger is usually constructed in a cross-flow arrangement, for convenience in air ducts sealing and separation of two air streams. Performance estimation has been a hot topic in this research. Zhang and Jiang [7], Zhang and Niu [8] have evaluated the system performance of the unit by heat and moisture transfer analysis. A correlation has been provided for effectiveness calculation, from Number of Transfer Units for heat transfer and moisture transfer [8]. According to the methodology, mean heat mass transfer coefficients between the air stream and the membrane surface are to be evaluated, with which and in combination with the resistance analysis through the membrane, sensible and moisture exchange effectiveness is calculated. Though simple, uncertainties may be high. In fact, the well-established Nusselt correlations, that were used for heat mass transfer coefficients estimation, were actually obtained either under uniform temperature or under uniform heat flux boundary conditions [9]. The real boundary conditions, however may deviate largely from such assumptions, especially for the current cross-flow exchanger that has strong heat mass transfer couplings between air streams and membrane materials.

A literature review found that similar problems also exist in heat and mass transfer analysis in other membrane-related technologies, such as gas–liquid contactor [10], pervaporation [11], distillation [12], extraction [13], etc. In fact, large deviations have been observed between the traditional heat transfer correlations and the experimental data on membrane surfaces [14]. Nevertheless, considerations of the effects of the real boundary conditions on the transport parameters are still scarce. To address this problem, in this study, the transport characteristics under real boundary conditions will be considered. This is a naturally formed boundary condition resulted from the interactions between the two flows, and the membrane.

2. The mathematical model

2.1. Governing equations

A schematic of the cross-flow enthalpy exchanger is shown in Fig. 1. The fresh air and the exhaust air flow through the passages in a cross-flow arrangement. Geometries of ducts: height $2a$, width $2b$, membrane thickness δ.

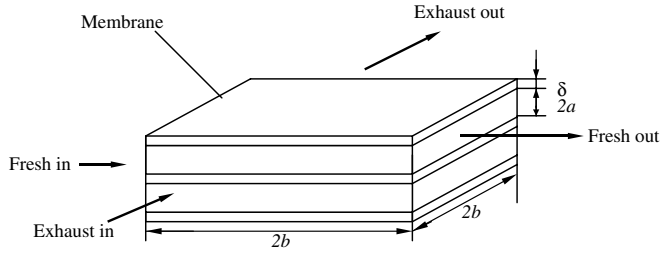

Fig. 1. Schematic of a cross-flow enthalpy exchanger with membrane cores.

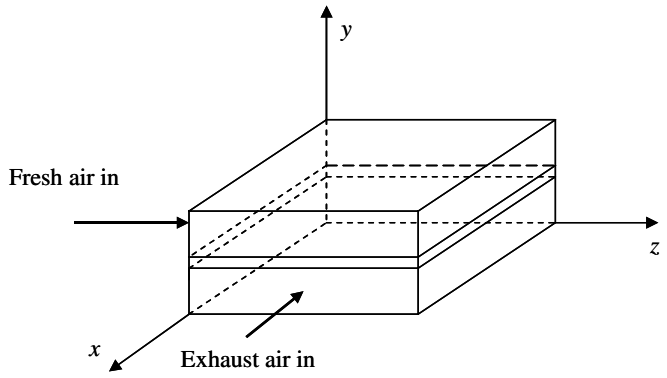

Fig. 2. The coordinate system of the unit showing one membrane and two neighboring flow passages.

The unit cell for model set-up is shown in Fig. 2. As plotted in the figure, the fresh air, which is usually hot and humid, flows along z-axis; while the exhaust air, which is usually cool and dry, flows inversely along the x-axis. Even though the coordinate system, inlet and boundaries conditions are different, the equations governing the transport phenomena are in the same form for the two passages. In the following, governing equations will be set-up for the fresh air. Then the different aspects for the exhaust flow will be pointed out. Both streams are flows in ducts of rectangular cross-sections. Flows in ducts have been investigated extensively by many researches, whether regular [15–18] or irregular cross-sections [19–24], but as mentioned before, influences of real boundary conditions were seldom considered. The issue will be investigated in this research.

In most applications, the Reynolds numbers are far below 2000, therefore it can be assumed laminar flow. It is considered to be hydrodynamically fully developed, but thermally developing. The fluid is Newtonian with constant thermal properties. Additional assumptions are: (1) adsorption of water vapor and membrane material is in equilibrium adsorption-state; (2) both the heat conductivity and the water diffusivity in the membrane are constants; (3) the heat of sorption is assumed constant and equal to the heat of vaporization.

2.1.1. Momentum conservation

For fully developed laminar flow in ducts, the Navier–Stokes equations reduce to [15,25]

$$\mu\left(\frac{\partial^2 u}{\partial x^2}+\frac{\partial^2 u}{\partial y^2}\right)=\frac{\mathrm{d}P}{\mathrm{d}z} \tag{1}$$

where μ is dynamic viscosity (Pa s), u is fluid velocity (m/s), P is the pressure (Pa), z is the axial coordinate (m).

2.1.2. Energy conservation

$$\rho c_p u\frac{\partial T}{\partial z}=\lambda\left(\frac{\partial^2 T}{\partial x^2}+\frac{\partial^2 T}{\partial y^2}\right) \tag{2}$$

where T is fluid temperature (K), λ is thermal conductivity (kW m^{-1} K^{-1}), (ρc_p) is heat capacity of moist air. It is calculated by the following equation as

$$\rho c_p=\rho_{\mathrm{a}}(c_{p\mathrm{a}}+\omega c_{p\mathrm{v}}) \tag{3}$$

where ρ_{a} is density of dry air (kg m^{-3}), $c_{p\mathrm{a}}$ and $c_{p\mathrm{v}}$ are specific heats of dry air and water vapor, respectively (kJ kg^{-1} K^{-1}), ω is humidity ratio (kg vapor/kg dry air).

2.1.3. Mass conservation

$$u\frac{\partial \omega}{\partial z}=D_{\mathrm{va}}\left(\frac{\partial^2 \omega}{\partial x^2}+\frac{\partial^2 \omega}{\partial y^2}\right) \tag{4}$$

where D_{va} is vapor diffusivity in dry air (m^2 s^{-1}).

2.2. Normalization of equations

The above three governing equations (1), (2) and (4) can be normalized as

$$\frac{\partial^2 u^*}{\partial x^{*2}}+\left(\frac{b}{a}\right)^2\frac{\partial^2 u^*}{\partial y^{*2}}+\frac{4b^2}{D_{\mathrm{h}}^2}=0 \tag{5}$$

$$U\frac{\partial \theta}{\partial z_{\mathrm{h}}^*}=\frac{\partial^2 \theta}{\partial x^{*2}}+\left(\frac{b}{a}\right)^2\frac{\partial^2 \theta}{\partial y^{*2}} \tag{6}$$

$$U\frac{\partial \xi}{\partial z_{\mathrm{m}}^*}=\frac{\partial^2 \xi}{\partial x^{*2}}+\left(\frac{b}{a}\right)^2\frac{\partial^2 \xi}{\partial y^{*2}} \tag{7}$$

where the dimensionless velocity is

$$u^*=-\frac{\mu u}{(\mathrm{d}P/\mathrm{d}z)D_{\mathrm{h}}^2} \tag{8}$$

and the dimensionless temperature is

$$\theta=\frac{T-T_{\mathrm{ci}}}{T_{\mathrm{hi}}-T_{\mathrm{ci}}} \tag{9}$$

where T_{hi} is the inlet temperature of the fresh air (hot and humid), and T_{ci} is the inlet temperature of the exhaust air (cool and dry).

Dimensionless humidity is

$$\xi=\frac{\omega-\omega_{\mathrm{ci}}}{\omega_{\mathrm{hi}}-\omega_{\mathrm{ci}}} \tag{10}$$

where ω_{hi} is the inlet humidity of the fresh air, and ω_{ci} is the inlet humidity of the exhaust air.

Dimensionless coordinates

$$x^* = \frac{x}{2b} \tag{11}$$

$$y^* = \frac{y}{2a} \tag{12}$$

$$z_h^* = \frac{z}{D_h RePr} \tag{13}$$

$$z_m^* = \frac{z}{D_h ReSc} \tag{14}$$

where hydraulic diameter

$$D_h = \frac{4A_c}{P_d} \tag{15}$$

where A_c is the cross-section area of the duct (m^2), P_d is the perimeter of the duct (m). Pr is Prandtl number, and Sc is Schmidt number. The dimensionless axis z^* has a different definition for heat transfer and mass transfer.

In Eqs. (6) and (7), velocity coefficient U is defined by

$$U = \frac{u^*}{u_m^*}\frac{4b^2}{D_h^2} \tag{16}$$

where u_m^* is the average dimensionless velocity on a cross-section, and it is calculated by

$$u_m^* = \frac{\int\int u^* \, dA}{A_c} \tag{17}$$

The characteristics of fluid flow in the duct can be represented by the product of the friction factor and the Reynolds number as

$$(fRe) = \left(-\frac{D_h \frac{dP}{dz}}{\frac{1}{2}\rho u_m^2}\right)\left(\frac{\rho u_m D_h}{\mu}\right) = \frac{2}{u_m^*} \tag{18}$$

Dimensionless bulk temperature

$$\theta_b(z_h^*) = \frac{\int\int u^* \theta \, dA}{\int\int u^* \, dA} \tag{19}$$

Dimensionless bulk humidity

$$\xi_b(z_m^*) = \frac{\int\int u^* \xi \, dA}{\int\int u^* \, dA} \tag{20}$$

Nusselt number

$$Nu = \frac{hD_h}{\lambda} \tag{21}$$

Sherwood number

$$Sh = \frac{kD_h}{D_{va}} \tag{22}$$

where h and k are convective heat transfer coefficient ($kW\,m^{-2}\,K^{-1}$) and convective mass transfer coefficient (m/s) between fluid and wall, respectively. The local Nusselt and Sherwood numbers may change from point to point on a duct surface. It is more practical to evaluate the peripherally mean local Nusselt and Sherwood numbers along the duct.

Considering the energy balance in a control volume of length Δz, heat transferred through convection

$$\dot{Q}_1 = h_L P_d \Delta z (T_W - T_b) \tag{23}$$

where h_L is the peripherally mean heat transfer coefficient, subscripts "w" and "b" refer to "wall" and "bulk", respectively. Enthalpy change of the fluid in the control volume

$$\dot{Q}_2 = \rho u_m A_c c_p \Delta T_b \tag{24}$$

Since

$$\dot{Q}_1 = \dot{Q}_2 \tag{25}$$

and

$$\Delta z = \Delta z_h^* D_h RePr = \Delta z_h^* \frac{\rho c_p u_m D_h^2}{\lambda} \tag{26}$$

the peripherally mean local heat transfer coefficient becomes

$$h_L = -\frac{1}{4(\theta_w - \theta_b)}\frac{\lambda}{D_h}\frac{\Delta\theta_b}{\Delta z_h^*} \tag{27}$$

Substituting above equation to Eq. (21), and considering the control volume to be infinitely small, then we obtain the peripherally local Nusselt number as

$$Nu_L = -\frac{1}{4(\theta_w - \theta_b)}\frac{d\theta_b}{dz_h^*} \tag{28}$$

Average Nusselt number from 0 to z_h^*

$$Nu_m = \frac{1}{z_h^*}\int_0^{z_h^*} Nu_L \, dz_h^* \tag{29}$$

Correspondingly, a mass balance on the control volume will have the following equations

$$k_L = -\frac{1}{4(\xi_w - \xi_b)}\frac{D_{va}}{D_h}\frac{\Delta\xi_b}{\Delta z_m^*} \tag{30}$$

$$Sh_L = -\frac{1}{4(\xi_w - \xi_b)}\frac{d\xi_b}{dz_m^*} \tag{31}$$

$$Sh_m = \frac{1}{z_m^*}\int_0^{z_m^*} Sh_L \, dz_m^* \tag{32}$$

As will be discussed later, the local Nusselt number and the local Sherwood number decrease asymptotically from very high values near the entrance of a tube to certain fully developed values at the end of thermal entry length. Under uniform temperature (uniform mass concentration) boundary condition, the fully developed value is denoted as Nu_T (Sh_T for mass). Under uniform heat flux (mass flux) boundary condition, it is denoted as Nu_H (Sh_H). In this study, under the real convective flow boundary conditions, the fully developed value is denoted as Nu_C (Sh_C for mass transfer).

2.3. Boundary conditions

The governing equations for the exhaust air stream are in the same form with the fresh air, however the coordinate systems are different. The membrane plate is a square one.

If we use x', y', z' to replace the coordinates x, y, z, in Eqs. (1)–(4), respectively, then we get the equations for the exhaust stream. The relations of the two coordinates systems are

$$\begin{cases} x' = z \\ y' = y \\ z' = 2b - x \end{cases} \tag{33}$$

Inlet conditions for fresh air

$$z_h^* = 0, \quad \theta = 1 \tag{34}$$

$$z_m^* = 0, \quad \xi = 1 \tag{35}$$

Inlet conditions for exhaust air

$$z_h^* = 0, \quad \theta = 0 \tag{36}$$

$$z_m^* = 0, \quad \xi = 0 \tag{37}$$

Boundary conditions of two air streams for velocity

$$u^* = 0, \quad \text{on all walls of the duct} \tag{38}$$

Temperature and humidity on wall surfaces are neither constant values nor constant fluxes. The flow is assumed to be hydrodynamically developed and thermodynamically and concentrationally developing. This means that the cross-sectional velocity field does not change with tube length, while the temperature and humidity fields vary with tube length. An analytical analysis of the boundary conditions on wall surfaces is difficult, if not impossible, due to the complexity in flow arrangement and interactions of temperature and humidity between the air streams and membrane materials. However, the boundary conditions on tube wall surfaces could be obtained numerically.

Adiabatic boundary conditions for fresh air

$$x^* = 0 \text{ or } x^* = 1, \quad \frac{\partial\theta}{\partial x^*} = \frac{\partial\xi}{\partial x^*} = 0 \tag{39}$$

and for exhaust air

$$x'^* = 0 \text{ or } x'^* = 1, \quad \frac{\partial\theta}{\partial x'^*} = \frac{\partial\xi}{\partial x'^*} = 0 \tag{40}$$

Temperature boundary conditions on membrane surfaces, for fresh air

$$y^* = 0 \text{ or } y^* = 1, \quad \theta(x^*, z_G^*) = \theta_{m1} \tag{41}$$

For exhaust air

$$y'^* = 0 \text{ or } y'^* = 1, \quad \theta(x'^*, z'^*_{G^*}) = \theta_{m2} \tag{42}$$

where term $\theta(x^*, z_{G^*})$ refers to air temperature adjacent to membrane surface at point (x^*, z_G^*), subscript "m" refers to membrane, and "1" and "2" refer to fresh side and exhaust side at the same point of membrane, respectively. Variable z_G^* is the dimensionless geometric position

$$z_G^* = \frac{z}{2b} \tag{43}$$

Due to the small thickness in membrane (100 μm, thermal conductivity 0.127 W m^{-1} K^{-1}), temperature differences between the two sides of a membrane are rather small. Heat released on the adsorption side of the membrane (fresh air side) could be balanced by the heat absorbed on the desorption side (exhaust side) of the membrane [26]. In fact, previous investigations disclosed that the temperature differences are in the order of 10^{-4} °C [27], meaning that Eqs. (41) and (42) can be expressed by a single equation by

$$\theta_{m1} = \theta_{m2} = \theta_m \tag{44}$$

The value of θ_m is not a fixed value. Rather, it is a result of local couplings between the two streams on membrane surface.

Mass boundary conditions on membrane surfaces, for fresh air

$$y^* = 0 \text{ or } y^* = 1, \quad q(x^*, z_{G^*}) = \dot{m}_v \tag{45}$$

For exhaust air

$$y'^* = 0 \text{ or } y'^* = 1, \quad q(x'^*, z'^*_{G^*}) = \dot{m}_v \tag{46}$$

where $\dot{m}_v$ (kg m^{-2} s^{-1}) is the moisture emission rate through membrane at point (x^*, z_G^*), and it is determined by diffusion equation in membrane as

$$\dot{m}_v = \rho_m D_{vm} \frac{W_{m1} - W_{m2}}{\delta} \tag{47}$$

where ρ_m and D_{vm} are density of membrane and moisture diffusivity in membrane, respectively. Variable W is water uptake in membrane (kg moisture/kg dry membrane), and it is expressed by a general sorption equation as

$$W = \frac{W_{max}}{1 - C + C/RH} \tag{48}$$

where W_{max} is the maximum water uptake of membrane material (kg/kg); C is a constant named the shape factor for the material; RH is air relative humidity. This sorption curve directly links water content to RH, a variable can be directly measured. The basic thermal physical parameters are obtained in the laboratory.

The relative humidity is calculated by humidity ratio and temperature as [28]

$$\frac{RH}{\omega} = \frac{e^{5294/T}}{10^6} - 1.61RH \tag{49}$$

where T is in K. The second term on the right side of the equation will generally have less than a 5% effect, and it can be usually neglected.

Moisture emission on membrane surface on fresh air or exhaust air side is calculated by

$$q = -\rho_a D_{va} \left.\frac{\partial\omega}{\partial y}\right|_{y=0,2a} \tag{50}$$

Similarly, emission rate q is not a constant value either. However, the values are attainable from couplings of Eqs. (41)–(46), plus governing equations (5)–(7).

2.4. Solution procedure

The partial differential equations for momentum, energy, and mass transport, Eqs. (5)–(7), are discretized

by means of a finite volume method. Since three components: two air streams and the membrane, are closely interacted, and temperature and humidity are also related to each other, iterative techniques are needed to solve these equations. A description of the iterative procedure is as following:

(a) Solve momentum equation Eq. (5) under the two coordinates systems and the two sets of inlet, and boundary conditions for the fresh air and the exhaust air stream. Get the velocity fields and resistance data for the two ducts.
(b) Assume initial temperature and humidity fields in the two streams. Get the membrane temperature.
(c) Solve energy equation Eq. (6) for the two streams, taking the current membrane temperatures as the boundary condition Eqs. (41) and (42), get the temperature fields in the two ducts.
(d) Calculate the new membrane surface temperature, by averaging the two ducts temperature at interfaces.
(e) Give the new membrane temperatures as the default values, and return to step (c), re-calculate the temperature fields of two air streams, until the old values and the newly calculated values for all temperatures are converged.
(f) Assume an initial emission rate through membrane.
(g) Based on the obtained temperature fields and boundary conditions of Eqs. (41) and (42), solve mass equation (7) under the two coordinate systems and the two sets of inlet conditions for the two air streams. Get the humidity fields in two ducts.
(h) Calculate the new emission rates through membrane, by equating Eqs. (47)–(50), from the newly calculated humidity fields in air streams.
(i) Give the new emission rates as the default values for emission rates, and return to step (g), until the old and new values of emission rates are converged.
(j) Check if all the new temperature, humidity, emission rates values are converged with old ones on all the calculating nodes. If not, return to step (c).

As seen, the whole procedure includes two loops: the temperature calculation loop from (b) to (e), and the humidity calculation loop from (f) to (i). The two loops form a bigger loop from (b) to (j), through which both humidity and temperature for all three components are calculated in a coupled way. The solution of velocity is only executed once before this big loop. A uniform initial guess is taken. The solution is insensitive to initial guesses. The solution of the discretized equations is by ADI iterations.

After these procedures, all the governing equations are satisfied simultaneously. The temperature and humidity profiles on membrane surfaces are the formed boundary conditions.

To assure the accuracy of the results presented, numerical tests were performed for the duct to determine the effects of the grid size. It indicates that 42×42 grids on cross-section and $\Delta z^* = 0.00025$ axially are adequate (less than 0.1% difference compared with 52×52 grids and $\Delta z^* = 0.000125$).

Table 1
Properties of the membrane used

Properties	Unit	Values
ρ_m	kg/m^3	836
D_{vm}	m^2/s	3.2×10^{-11}
δ	μm	100
W_{max}	kg/kg	0.27
C		0.81

2.5. Membrane properties

As pointed out before, membrane materials have an impact on the coupled heat mass transfer phenomena. The influences mainly come from its resistance on moisture transfer. Both temperature and humidity will affect the water uptake in membrane. Membranes that are permeable to water vapor, but not to air, is the criteria for selection. In this study, a dense AC (acetate cellulose) membrane with which we have much experience from previous studies is selected. The tested thermodynamic properties are listed in Table 1. The nominal inlet conditions: fresh air 35 °C and 0.025 kg/kg; exhaust air 25 °C and 0.010 kg/kg.

3. Results and discussion

3.1. Velocity and friction factor

The flow profiles in the two passages are identical. The velocity contours on duct cross-section is plotted in Fig. 3 for an aspect ratio of $b/a = 4.0$. The boundaries have influences on the shapes of contours. In the duct center, the contours are elliptical in shape, but in place near wall, the contours are more like rectangles. In the four corners, there are dead spaces where velocity is near zero. This will cause heat and mass transfer to deteriorate.

For hydrodynamically fully developed laminar flow in ducts, (fRe) is a constant. The calculated values of (fRe) for various aspect ratios are listed in Table 2. A compari-

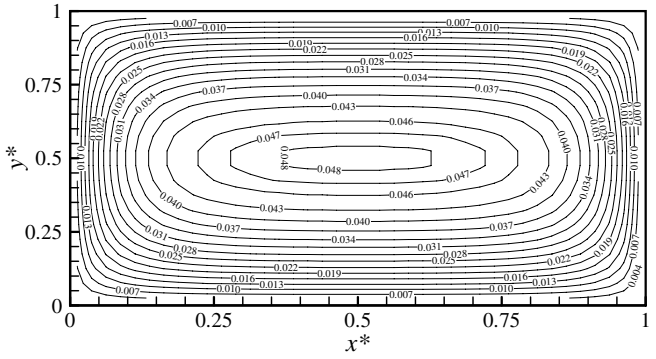

Fig. 3. Contours of dimensionless velocity (u^*) in the duct.

Table 2
Fully developed (fRe) and Nusselt, Sherwood numbers for various aspect ratios

b/a	Nu_H	Nu_T	Nu_C	Sh_C	(fRe)	(fRe)
Sources	Ref. [9,15]	Ref. [9,15]	(This study)	(This study)	Ref. [9,15]	(This study)
1.0	3.61	2.98	1.88	1.89	57.0	56.58
1.43	3.73	3.08	2.49	2.52	59.0	58.09
2.0	4.12	3.39	3.06	3.10	62.0	61.83
3.0	4.79	3.96	4.06	4.00	69.0	68.09
4.0	5.33	4.44	4.64	4.52	73.0	72.45
8.0	6.49	5.60	6.06	6.03	82.0	81.66
50.0			7.78	7.81		92.39
100.0			8.07	8.05		93.92
∞	8.23	7.54			96.0	

son is also made with the values form well-known Refs. [9,15,25]. As seen, the current study predicts the flow well. The maximum deviation is less than 1.5%. The flow resistance is independent of the naturally formed boundary conditions. They are in accordance with the published data.

In the following, the calculations will be conducted for a parallel plate with an aspect ratio of 50. Reynolds numbers change from 50 to 500, since they are typical for our test.

3.2. Temperature and Nusselt numbers

The bulk temperature of the two air streams along the flow direction is plotted in Fig. 4. Peripherally mean temperature of duct walls (membrane) is also shown in the figure. "Temperature membrane mean 1" is averaged perpendicularly to z-axis, while "temperature membrane mean 2" is averaged perpendicularly to $-x$ axis. As seen, the fresh air temperature decreases while the flow propagating. The exhaust air temperature rises when moving forward. The membrane temperature changes with the stream passing by: it decreases with fresh air temperature, and it rises with increasing exhaust air temperature. Since heat is transferred from the fresh to the exhaust, "membrane 2" temperature is higher than the exhaust stream.

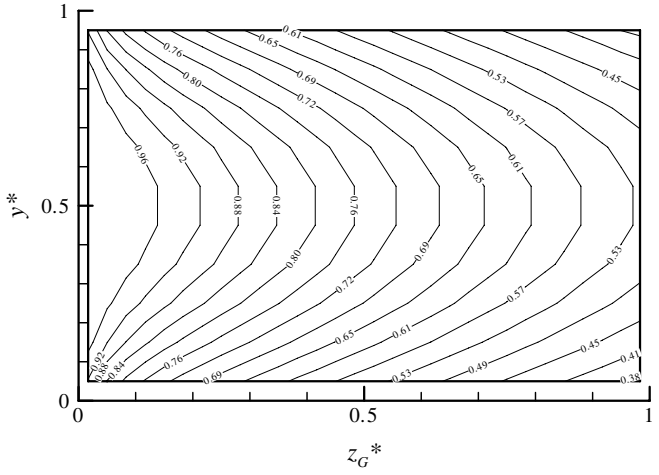

Fig. 5. Dimensionless temperature profiles in y–z plane at $x^* = 0.5$ for fresh air.

The dimensionless temperature profiles in y–z plane at $x^* = 0.5$ are plotted in Fig. 5 for fresh air. Axis z represents the flow direction for the two flows. As seen, the profiles are symmetric, similar to flows in traditional ducts.

The peripherally local and mean Nusselt numbers along the flow direction for any one of the two streams are drawn in Fig. 6. Due to the increasing thickness in thermal boundary layers, the local Nusselt number will decrease and approach asymptotically to a lower limiting value with the marching of flow. After that period, the flow is called the thermally developed region. This lower limiting value of Nusselt number is denoted as Nu_C, in comparison with Nu_T under uniform temperature boundary condition and Nu_H under uniform heat flux boundary condition, from other famous works [15,25]. After $z_h^* = 0.15$, the flow can

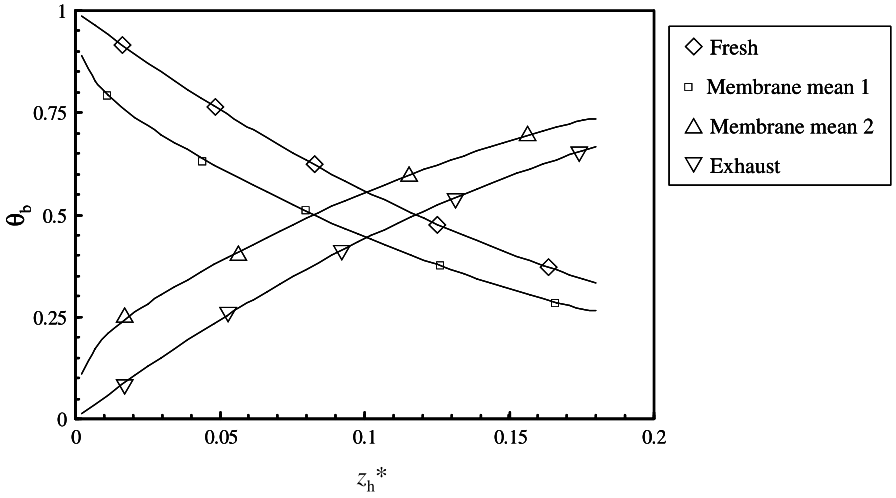

Fig. 4. Bulk temperature of two fluids and the mean temperature of the membrane along flow direction. Membrane mean 1: peripheral mean for fresh air; membrane mean 2: peripheral mean for exhaust air.

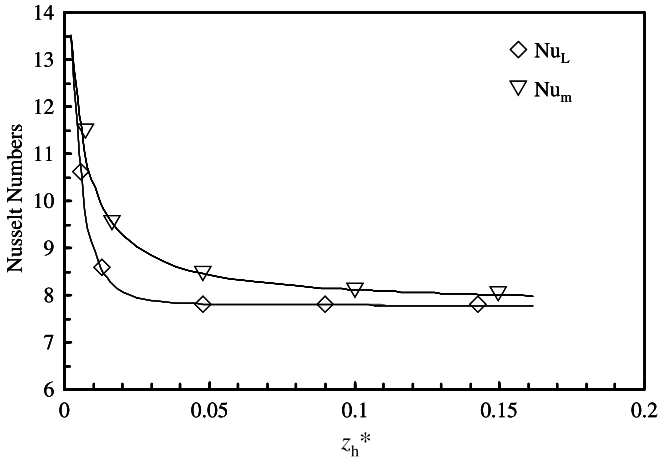

Fig. 6. Local and mean Nusselt numbers along flow direction, $b/a = 50$.

be considered as thermally fully developed. At this point, $z = 2$ cm. Therefore the duct is long enough (5 cm) for flow to get fully developed.

The detailed values of Nu_C for various aspect ratios are listed in Table 2. For comparison, the values of Nu_T and Nu_H are also listed. A comparison between Nu_C, Nu_T and Nu_H are plotted in Fig. 7. As seen from this figure, Nu_H is usually 20% larger than Nu_T. Nu_C is generally less than Nu_H. It is higher than Nu_T at larger aspect ratios, but 37% less than Nu_T at smaller aspect ratios. For parallel plates that have large aspect ratios, in engineering applications, Nu_C can be approximated by Nu_T. It can also be found that at low aspect ratios, Nu_H and Nu_T reach a steady value where as Nu_C continue to decrease with decrease in aspect ratios, the reason is that for this exchanger, the heat and mass transfer is coupled. Under low aspect ratios, the coupling effect will make the transfer deteriorate.

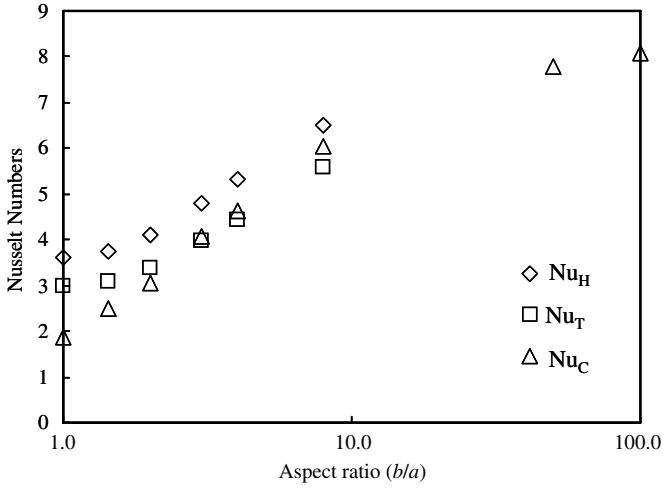

Fig. 7. Fully developed Nusselt numbers for cross-flow ducts, and in comparison with those under uniform temperature and uniform heat flux boundary conditions.

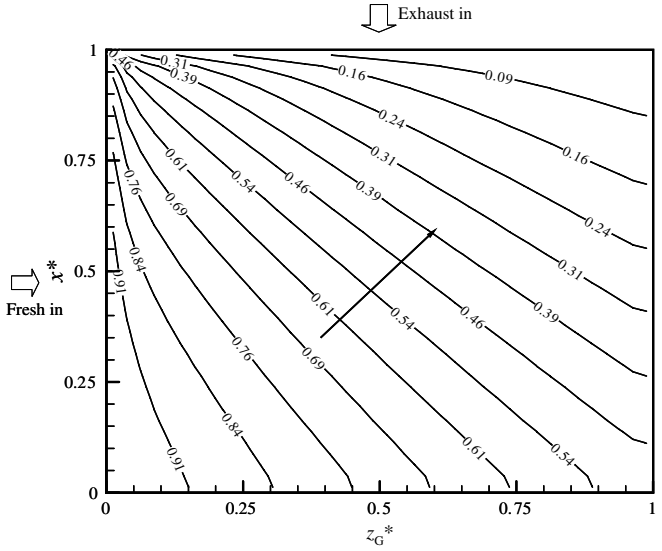

Fig. 8. Dimensionless surface temperature contours on membrane in the cross-flow exchanger, the arrow in the figure showing direction of contours value decreasing.

Now it's interesting to study the temperature profiles on membrane surface. They are the real boundary conditions for temperature. The dimensionless temperature contours are shown in Fig. 8 and the contours of heat flux (W/m^2) through the membrane are shown in Fig. 9. It is clear that the boundary condition is neither uniform temperature nor uniform heat flux surfaces. Both the temperature and the heat flux exhibit a non-uniform two-dimensional behavior. The directions for temperature and heat flux decreasing are parallel to the diagonal line of the square.

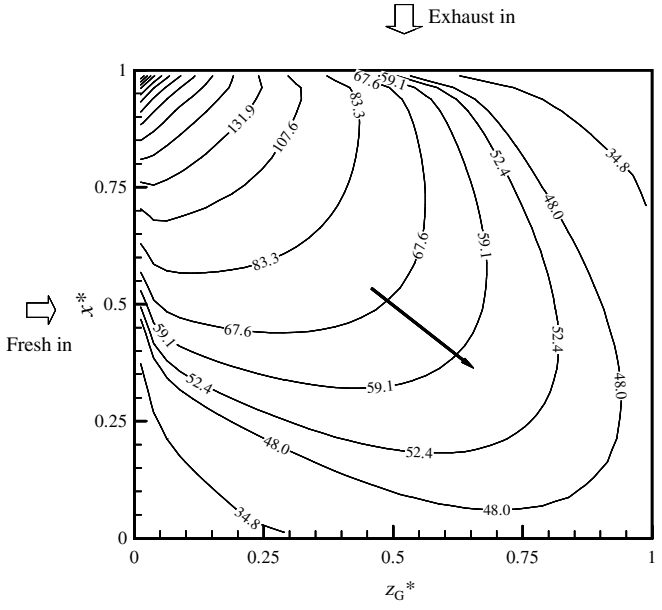

Fig. 9. Surface heat flux contours through the membrane in the cross-flow exchanger (W/m^2), the arrow showing the direction of heat flux contour values decreasing.

3.3. Humidity and Sherwood numbers

Transport of humidity in two ducts is similar to temperature. Distinct differences lie in the fact that the humidity profiles on the two surfaces of membrane are different, indicating that mass resistance through membrane is substantial. The calculated dimensionless humidity on membrane surface is shown in Fig. 10 on fresh air side and in Fig. 11 on exhaust air side, respectively. They also show a two-dimensional distributed nature. The contour lines are parallel to the diagonal line. The surface values are non-uniform concentration boundaries. Even on the same surface, the concentration values change largely: the highest concentrations are 5.7 times and 8.7 times higher than the least concentrations on fresh air side and exhaust air side, respectively.

The moisture emission rates (mass fluxes) through the membrane are shown in Fig. 12. Under current situation, mass fluxes range from 1.7×10^{-4} to 5.0×10^{-5} kg m^{-2} s^{-1}. The maximum differences in values are 3.4 times. The contour values decrease along the diagonal line like a ripple in a pool, whose center is at the point where the two flows intersect and enter the exchanger.

From above discussions, it indicates that the humidity boundaries are neither uniform concentration nor uniform mass flux boundary conditions. Fig. 13 shows the bulk humidity along the dimensionless axis and the peripherally mean membrane humidity profiles. Dimensionless humidity profiles in the air stream in y–z plane at $x^* = 0.5$ for the fresh air is plotted in Fig. 14

Fig. 15 shows the local and mean Sherwood numbers along the flow for any one of the two streams. The variations of the bulk flow and the Sherwood numbers are similar to bulk temperature and Nusselt numbers. In the concentration developing region, the local Sherwood numbers decrease sharply, from a high value to a lower limiting value denoted as Sh_C. The flow is called concentrationally developed after that period. The calculated Sh_C for various aspect ratios are also listed in Table 2. It is found that $Sh_C \approx Nu_C$ for most aspect ratios. The developing length is satisfied by $z_m^* \approx z_h^*$.

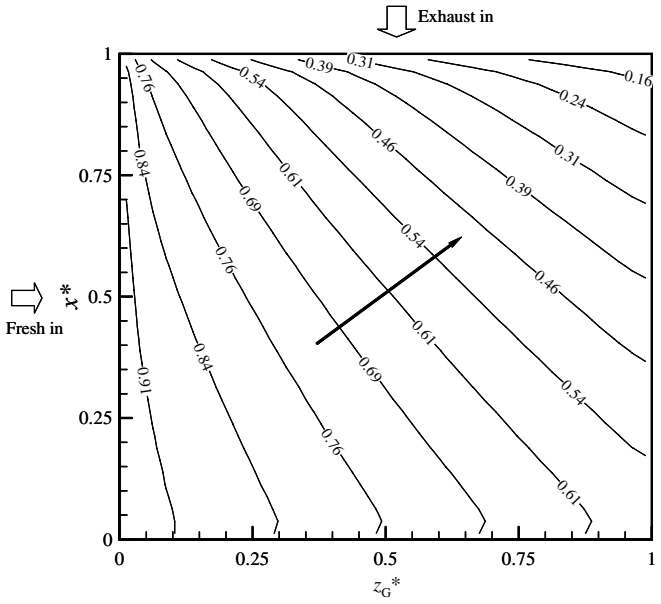

Fig. 10. Contours of dimensionless surface humidity on fresh air side in the cross-flow exchanger, the arrow in the figure showing direction of contours value decreasing.

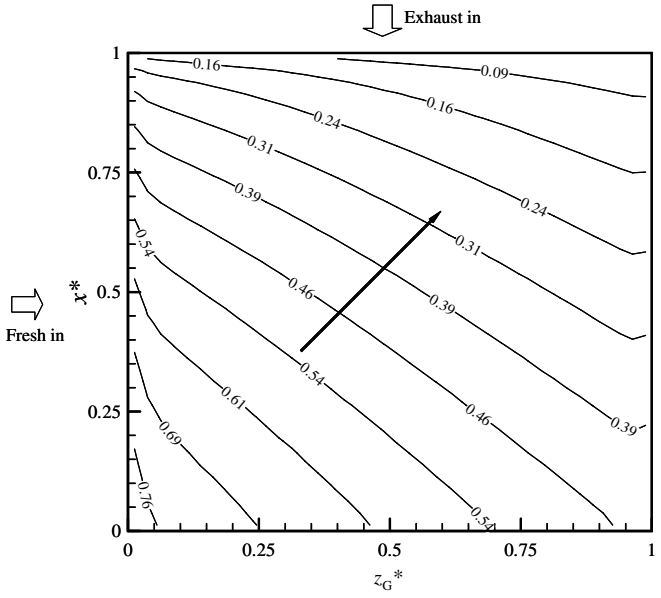

Fig. 11. Contours of dimensionless surface humidity on exhaust air side in the cross-flow exchanger, the arrow in the figure showing direction of contours value decreasing.

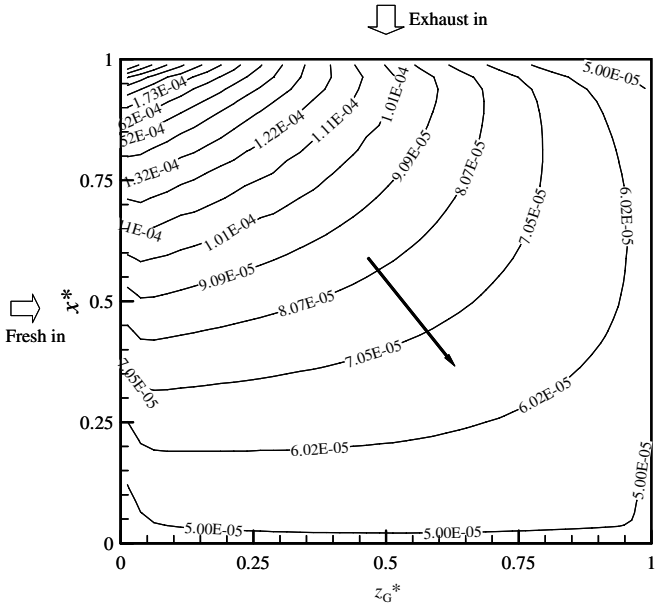

Fig. 12. Mass flux contours through the membrane in the cross-flow exchanger (kg m^{-2} s^{-1}), the arrow in the figure showing the direction of contours value decreasing.

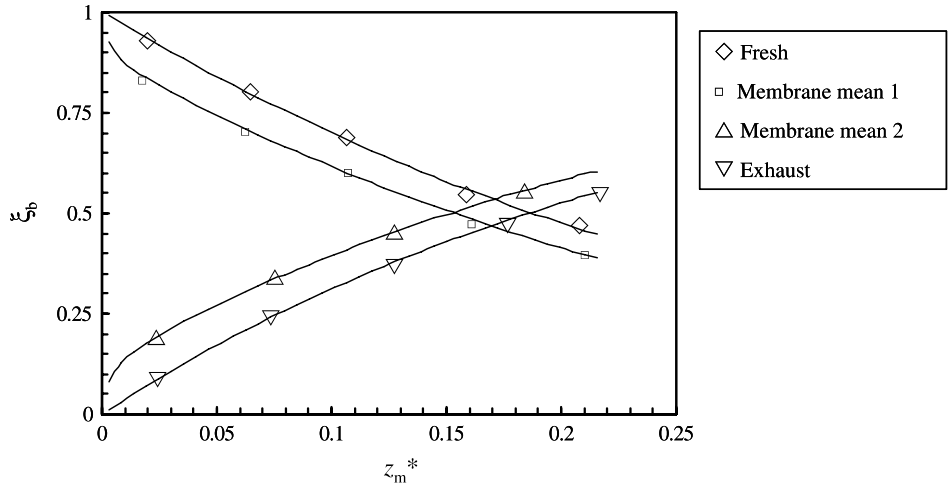

Fig. 13. Bulk humidity of two fluids and the mean surface humidity of the membrane along flow direction. Membrane mean 1: peripheral mean along fresh air; membrane mean 2: peripheral mean along exhaust air.

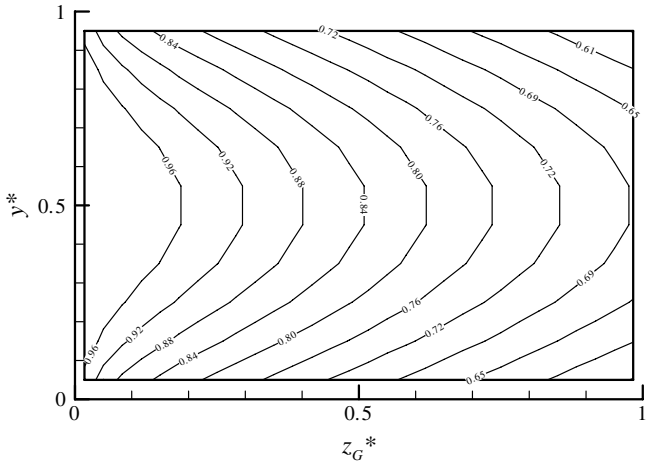

Fig. 14. Dimensionless humidity profiles in y–z plane at $x^* = 0.5$ for fresh air.

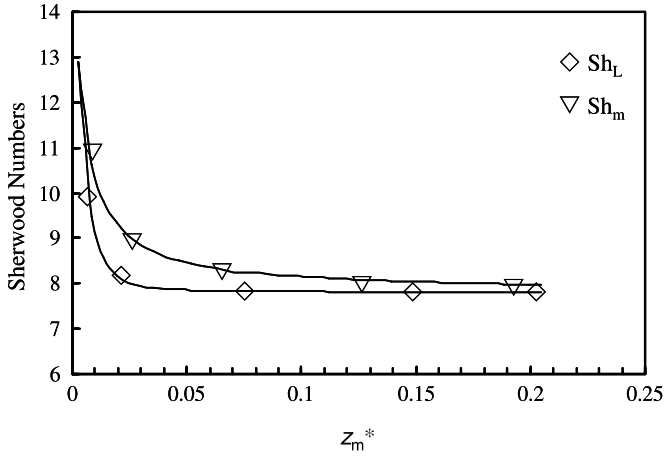

Fig. 15. Local and mean Sherwood numbers along flow direction, $b/a = 50$.

3.4. Experimental work

An experimental set-up has been built to study the heat and mass transport in a membrane-based cross-flow exchanger. The whole set-up is shown in Fig. 16. Ambient air is humidified and is driven to a heating/cooling coil in a hot/cool water bath. The cooling coil can also act as dehumidifier when required. After the temperature and humidity reach the set points, it is then drawn through the exchanger for heat and moisture exchange. Another flow is driven directly from ambient to the exchanger. An AC membrane is sandwiched by two stainless steel shell, which forms an air passage on both sides of membrane, like a one-plate plate-and-shell heat exchanger. The passage dimensions are $2b = 10$ cm, $2a = 2$ mm. During the experiment, air flow rate is changed, to have different Reynolds numbers. Humidity, temperature, and volumetric flow rates are monitored at the inlet and outlet of the exchanger. Equal air flow rates are kept for the two streams. The uncertainties are: temperature ±0.1 °C; humidity ±1%; volumetric flow rate ±0.5%.

During the experiment, energy balance and mass balance are checked. Energy balance found that even though active insulation measures have been taken, there is still more than 20% of inputted thermal energy that is dissipated to the surroundings through the stainless steel shell. So currently, we did not use the measured temperature for results analysis. However, mass balance is satisfied, and the difference of moisture content between the input and the output is within 2% limit. The relations between heat and mass transfer can be expressed by the Chilton–Colburn analogy [28], namely

$$Sh = Nu \cdot Le^{-1/3} \tag{51}$$

$$Le = \frac{Pr}{Sc} \tag{52}$$

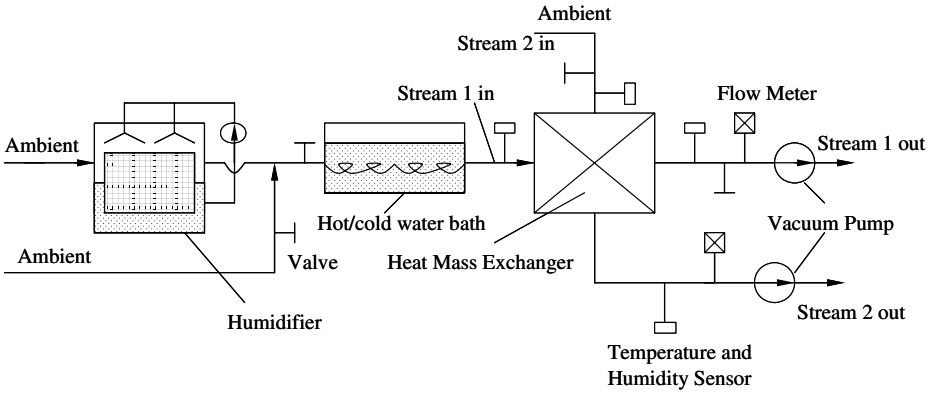

Fig. 16. Experimental set-up.

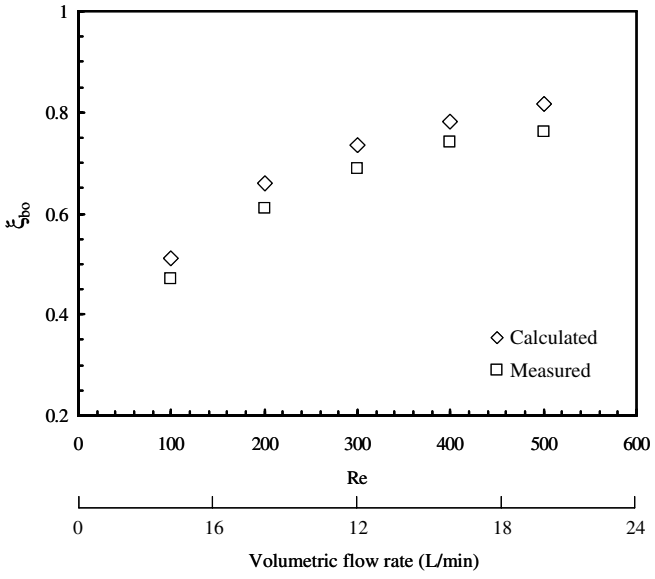

Fig. 17. Dimensionless outlet bulk humidity of fresh air from the exchanger.

where *Le* is commonly called the Lewis number. From this analogy, *Sh* can be estimated from *Nu*, and vice versa.

The measured outlet dimensionless bulk humidity for fresh air is shown in Fig. 17 for various air flow rates. The calculated values from the above model are also plotted in the figure. Generally the two sets of data fit well. The maximum deviation is below 7.8%. The boundary condition at $y^* = y'^* = 1$ has been revised to have zero flux, to reflect the one-plate nature in the model.

4. Conclusions

For a cross-flow heat mass exchanger that has membrane cores, the boundary conditions are numerically obtained by the simultaneous solution of momentum, energy, and concentration equations of two flows and their couplings with membrane. The naturally formed heat and mass boundary conditions are neither uniform flux nor uniform value boundary conditions. Whether it's heat flux (mass flux) or temperature (concentration) on membrane surface, the values exhibit a distinct two-dimensional distributed nature. The flow is developing both thermally and concentrationally when they enter the exchanger. Lower limiting values of local Nusselt and Sherwood numbers are obtained after the flow becomes fully developed.

The fully developed Nusselt number Nu_C is generally less than Nu_H. It is higher than Nu_T at larger aspect ratios, but 37% less than Nu_T at smaller aspect ratios. For parallel plates that have large aspect ratios, Nu_C can be approximated by Nu_T. The fully developed Sherwood numbers are nearly equal to the fully developed Nusselt numbers. This gives some insight for future applications.

Acknowledgements

This Project is jointly supported by National Natural Science Foundation of China (50306005), Fok Ying Tung Education Foundation (101057), and Natural Science Foundation of Guangdong Province (05006557).

References

[1] ASHRAE, ASHRAE Handbook-Fundamentals, American Society of Heating, Refrigerating, and Air-Conditioning Engineers Inc., Atlanta, 1999.
[2] X.P. Wu, P. Johnson, A. Akbarzadeh, Application of heat pipe heat exchangers to humidity control in air-conditioning systems, Appl. Therm. Eng. 17 (6) (1997) 561–568.
[3] F.J.R. Martinez, M.A.A.G. Plasencia, E.V. Gomez, F.V. Diez, R.H. Martin, Design and experimental study of a mixed energy recovery system, heat pipes and indirect evaporative equipment for air conditioning, Energy Build. 35 (10) (2003) 1021–1030.
[4] J.Y. San, Heat and mass transfer in a two-dimensional cross-flow regenerator with a solid conduction effect, Int. J. Heat Mass Transfer 36 (1993) 633–643.
[5] C.J. Simonson, R.W. Besant, Energy wheel effectiveness: Part I—Development of dimensionless groups, Int. J. Heat Mass Transfer 42 (1999) 2161–2170.
[6] K.R. Kistler, E.L. Cussler, Membrane modules for building ventilation, Chem. Eng. Res. Des. 80 (2002) 53–64.
[7] L.Z. Zhang, Y. Jiang, Heat and mass transfer in a membrane-based energy recovery ventilator, J. Membr. Sci. 163 (1999) 29–38.

[8] L.Z. Zhang, J.L. Niu, Effectiveness correlations for heat and moisture transfer processes in an enthalpy exchanger with membrane cores, ASME J. Heat Transfer 122 (5) (2002) 922–929.
[9] F.P. Incropera, D.P. Dewitt, Introduction to Heat Transfer, third ed., John Wiley & Sons, New York, 1996, p. 416 (Chapter 8).
[10] V.Y. Dindore, G.F. Versteeg, Gas–liquid mass transfer in a cross-flow hollow fiber module: Analytical model and experimental validation, Int. J. Heat Mass Transfer 48 (2005) 3352–3362.
[11] S. Sommer, B. Klinkhammer, M. Schleger, T. Melin, Performance efficiency of tubular inorganic membrane modules for pervaporation, AIChE J. 51 (1) (2005) 162–177.
[12] B. Li, K.K. Sirkar, Novel membrane and device for vacuum membrane distillation-based desalination process, J. Membr. Sci. 257 (2005) 60–75.
[13] H.M. Yeh, Y.K. Chen, Membrane extraction through cross-flow rectangular modules, J. Membr. Sci. 170 (2000) 235–242.
[14] J.I. Mengual, M. Khayet, M.P. Godino, Heat and mass transfer in vacuum membrane distillation, Int. J. Heat Mass Transfer 47 (2004) 865–875.
[15] R.K. Shah, A.L. London, Laminar Flow Forced Convection in Ducts, Academic Press Inc., New York, 1978.
[16] D.F. Sherony, C.W. Solbrig, Analytical investigation of heat or mass transfer and friction factors in a corrugated duct heat or mass exchanger, Int. J. Heat Mass Transfer 13 (1970) 145–159.
[17] L. Fischer, H. Martin, Friction factors for fully developed laminar flow in ducts confined by corrugated parallel walls, Int. J. Heat Mass Transfer 40 (1997) 635–639.
[18] Z.F. Dong, M.A. Ebadian, A numerical analysis of thermally developing flow in elliptic ducts with internal fins, Int. J. Heat Fluid Flow 12 (1991) 166–172.
[19] M.A. Ebadian, H.Y. Zhang, Fluid flow and heat transfer in the crescent-shaped lumen catheter, ASME J. Appl. Mech. 60 (1993) 721–727.
[20] R.K. Shah, Laminar flow friction and forced convection heat transfer in ducts of arbitrary geometry, Int. J. Heat Mass Transfer 18 (1975) 849–862.
[21] T. Yilmaz, E. Cihan, General equation for heat transfer for laminar flow in ducts of arbitrary cross-sections, Int. J. Heat Mass Transfer 36 (1993) 3265–3270.
[22] T. Yilmaz, General equation for pressure drop for laminar flow in ducts of arbitrary cross-sections, ASME J. Energy Resourc. Technol. 112 (1990) 220–223.
[23] J.L. Niu, L.Z. Zhang, Heat transfer and friction coefficients in corrugated ducts confined by sinusoidal and arc curves, Int. J. Heat Mass Transfer 45 (3) (2001) 571–578.
[24] L.Z. Zhang, J.L. Niu, A numerical study of laminar forced convection in sinusoidal ducts with arc lower boundaries under uniform wall temperature, Numer. Heat Transfer, Part A: Applications 40 (1) (2001) 55–72.
[25] W.M. Kays, M.E. Crawford, in: Convective Heat and Mass Transfer, McGraw-Hill, Inc., New York, 1993, pp. 75–87.
[26] L.Z. Zhang, Y. Jiang, Y.P. Zhang, Membrane-based humidity pump: performance and limitations, J. Membr. Sci. 171 (2) (2000) 207–216.
[27] E. Favre, Temperature polarization in pervaporation, Desalination 154 (2003) 129–138.
[28] J.L. Niu, L.Z. Zhang, Membrane-based enthalpy exchanger: material considerations and clarification of moisture resistance, J. Membr. Sci. 189 (2001) 179–191.